European Journal of Mechanics A/Solids 63 (2017) 43–52

Contents lists available at ScienceDirect

European Journal of Mechanics A/Solids

journal homepage: www.elsevier.com/locate/ejmsol

On the analysis of pure bending of rigid-plastic beams in strain-gradient plasticity

Vlado A. Lubarda [a, b]

[a] Department of NanoEngineering, University of California, San Diego, La Jolla, CA 92093-0448, USA
[b] Department of Mechanical and Aerospace Engineering, University of California, San Diego, La Jolla, CA 92093-0411, USA

ARTICLE INFO

Article history:
Received 21 December 2015
Received in revised form
17 November 2016
Accepted 1 December 2016
Available online 19 December 2016

Keywords:
Beam bending
Line forces
Material length parameter
Microstress
Moment-stress
Strain-gradient plasticity
Moment-curvature relationship
Rigid-plastic

ABSTRACT

The complete stress field, including the microstress, the moment-stress, and the line forces are derived for the pure bending of a rigid-plastic beam of rectangular cross-section in the model of strain-gradient plasticity. The workless spherical parts of the microstress and the moment-stress tensors are incorporated in the analysis. Their determination is shown to be of importance for the fulfilment of the higher-order traction boundary conditions, the physical interpretation of line forces, and their contributions to bending moments. Three equivalent methods are used to derive the moment-curvature relationship for any of the gradient-enhanced effective plastic strain measures from the considered broad class of these measures. Specific results are given for the selected choice of the stress-strain relationship describing the uniaxial tension test. Closed-form analytical expressions are obtained in the case of linear hardening, and in some cases of nonlinear hardening. The analysis of the plane-strain bending of thin foils is also presented. In this case there are two sets of line forces along the edges of the beam. The relationships between the applied bending moment and the curvature, and between the lateral bending moment and the curvature are derived and discussed. The lateral bending moment along the lateral sides of the beam, needed to keep the plane-strain mode of deformation, is one-half of the applied bending moment.

1. Introduction

In the strain-gradient plasticity theory the microstress and the moment-stress are the deviatoric tensors introduced as the work-conjugates to the deviatoric plastic strain tensor and its gradient (Fleck and Hutchinson, 1997, 2001; Gudmundson, 2004; Anand et al., 2005; Gurtin and Anand, 2005, 2009; Bardella, 2006; Fleck and Willis, 2009; Hutchinson, 2012; Nielsen and Niordson, 2014; Fleck et al., 2014, 2015; Lubarda, 2016a). We show in this paper through the analysis of pure bending of a rigid-plastic beam that it is important to incorporate in the analysis the (workless) spherical parts of the microstress and the moment-stress tensors, in addition to their deviatoric parts. This allows the fulfilment of the higher-order traction boundary conditions, the interpretation of the line forces along the intersection of the bounding surfaces of the beam, and the evaluation of the (reactive) lateral bending moment in the case of plane-strain bending. In Sections 2–4 we present a brief review of the J_2 deformation theory of strain-gradient plasticity by using an arbitrary measure of the gradient-enhanced effective plastic strain from a wide class of these measures introduced in the literature (Fleck and Hutchinson, 1997, 2001). The stress fields in a rigid-plastic beam of rectangular cross-section under pure bending are derived in Section 5. The deviatoric pats are determined by usual means from the established constitutive equations, while the spherical parts are determined by the fulfilment of the higher-order traction boundary conditions. Three equivalent methods are used in Section 6 to derive the moment-curvature relationship for any of the utilized gradient-enhanced effective plastic strain measures. Closed-form analytical expressions are obtained in the case of linear hardening, and for some measures of the effective plastic strain in the case of nonlinear hardening. For an adopted nonlinear stress-strain relationship describing the uniaxial tension test, the moment-curvature relationships are evaluated numerically in Section 7. The analysis of the plane-strain model of the bending of a wide rigid-plastic beam is presented in Section 8, since such model has been commonly adopted in the bending analysis of thin foils (Stölken and Evans, 1998; Huang et al., 2000; Wang et al., 2003; Haque and Saif, 2003; Voyiadjis and Abu Al-Rub, 2005; Engelen et al., 2006; Lou et al., 2006; Evans and Hutchinson, 2009; Idiart

E-mail address: vlubarda@ucsd.edu.

http://dx.doi.org/10.1016/j.euromechsol.2016.12.001
0997-7538/

et al., 2009). Two types of line forces are shown to act along different edges of the beam. They are used to derive the applied bending moment-curvature and the lateral bending moment-curvature relationships. The lateral stresses are shown to be equal to one-half of the corresponding longitudinal stresses. As a consequence, the lateral bending moment (per unit length of the beam) is equal to one-half of the applied bending moment (per unit width of the beam).

2. Gradient-enhanced effective plastic strain

In a simple formulation of the deformation theory of strain-gradient plasticity (Hutchinson, 2012), the specific plastic work (per unit volume) is expressed in terms of the gradient-enhanced effective plastic strain E_{p} by

$$w_{\mathrm{p}}(E_{\mathrm{p}}) = \int_0^{E_{\mathrm{p}}} \sigma_0(\varepsilon_{\mathrm{p}})\, \mathrm{d}\varepsilon_{\mathrm{p}}, \tag{1}$$

where $\sigma_0 = \sigma_0(\varepsilon_{\mathrm{p}})$ represents the stress-strain curve from the uniaxial tension test. A wide class of the gradient-enhanced effective plastic strain measures, each involving one (albeit possibly different) material length parameter l (Fleck and Hutchinson, 1997; Evans and Hutchinson, 2009), is

$$E_{\mathrm{p}} = \left(e_{\mathrm{p}}^s + l^s g_{\mathrm{p}}^s\right)^{1/s}, \quad (s \geq 1)\,. \tag{2}$$

Here, e_{p} is the effective plastic strain and g_{p} the effective plastic strain-gradient, defined by

$$e_{\mathrm{p}} = \left(\frac{2}{3}\varepsilon_{ij}^{\mathrm{p}}\varepsilon_{ij}^{\mathrm{p}}\right)^{1/2}, \quad g_{\mathrm{p}} = \left(\frac{2}{3}\varepsilon_{ij,k}^{\mathrm{p}}\varepsilon_{ij,k}^{\mathrm{p}}\right)^{1/2}. \tag{3}$$

The two most frequently used measures are associated with the choices $s = 1$ and $s = 2$, which specify E_{p} as either a linear or harmonic sum of e_{p} and lg_{p}, i.e.,

$$E_{\mathrm{p}} = e_{\mathrm{p}} + l g_{\mathrm{p}}\,, \quad E_{\mathrm{p}} = \left(e_{\mathrm{p}}^2 + l^2 g_{\mathrm{p}}^2\right)^{1/2}. \tag{4}$$

The plastic strain is taken to be

$$\varepsilon_{ij}^{\mathrm{p}} = e_{\mathrm{p}} m_{ij}\,, \quad m_{ij} = \frac{3}{2}\frac{\sigma'_{ij}}{\sigma_{\mathrm{eq}}}\,, \tag{5}$$

with the equivalent stress

$$\sigma_{\mathrm{eq}} = \left(\frac{3}{2}\sigma'_{ij}\sigma'_{ij}\right)^{1/2}, \tag{6}$$

where prime designates the deviatoric part.

The total infinitesimal strain ε_{ij} is the sum of elastic and plastic contributions. For the rigid-plastic material model of concern in this paper, the elastic component is absent, so that $\varepsilon_{ij} = \varepsilon_{ij}^{\mathrm{p}}$.

3. Work-conjugates to plastic strain and its gradient

It is assumed that the plastic strain-gradients $\varepsilon_{ij,k}^{\mathrm{p}}$ contribute to the work per unit volume. The work conjugate to $\varepsilon_{ij,k}^{\mathrm{p}}$ is the moment-stress $\tau_{ijk} = \tau_{jik}$, and the work-conjugate to $\varepsilon_{ij}^{\mathrm{p}}$ is the microstress $q_{ij} = q_{ji}$, such that (Gudmundson, 2004)

$$\dot{w}_{\mathrm{p}} = q_{ij}\dot{\varepsilon}_{ij}^{\mathrm{p}} + \tau_{ijk}\dot{\varepsilon}_{ij,k}^{\mathrm{p}}\,. \tag{7}$$

Since $\varepsilon_{kk}^{\mathrm{p}} = 0$, only the deviatoric parts of q_{ij} and τ_{ijk} contribute to plastic work. To identify them, we evaluate the rate of plastic work from (1) as

$$\dot{w}_{\mathrm{p}} = \sigma_0(E_{\mathrm{p}})\dot{E}_{\mathrm{p}}\,. \tag{8}$$

By the differentiation of (2) and (3), the rate of the gradient-enhanced effective plastic strain is found to be

$$\dot{E}_{\mathrm{p}} = \frac{2}{3}E_{\mathrm{p}}^{1-s}\left(e_{\mathrm{p}}^{s-2}\varepsilon_{ij}^{\mathrm{p}}\dot{\varepsilon}_{ij}^{\mathrm{p}} + l^s g_{\mathrm{p}}^{s-2}\varepsilon_{ij,k}^{\mathrm{p}}\dot{\varepsilon}_{ij,k}^{\mathrm{p}}\right). \tag{9}$$

The substitution of (9) into (8), and the comparison with (7), establishes the constitutive expressions for the deviatoric parts

$$q'_{ij} = \frac{2}{3}\frac{\sigma_0(E_{\mathrm{p}})}{E_{\mathrm{p}}^{s-1}}\, e_{\mathrm{p}}^{s-2}\varepsilon_{ij}^{\mathrm{p}}\,, \quad \tau'_{ijk} = \frac{2}{3}l^s\frac{\sigma_0(E_{\mathrm{p}})}{E_{\mathrm{p}}^{s-1}}\, g_{\mathrm{p}}^{s-2}\varepsilon_{ij,k}^{\mathrm{p}}\,. \tag{10}$$

The spherical parts of q_{ij} and τ_{ijk} do not contributing to the plastic work, and at this point of the analysis are arbitrary. If needed, however, they may be specified by the consideration of the higher-order traction boundary conditions, as discussed in Section 5.1 in the context of the rigid-plastic beam bending.

4. Principle of virtual work

In the case of a rigid-plastic body of volume V, bounded by a piece-wise smooth surface S, the principle of virtual work is

$$\int_V \left(q'_{ij}\delta\varepsilon_{ij}^{\mathrm{p}} + \tau'_{ijk}\delta\varepsilon_{ij,k}^{\mathrm{p}} + \frac{1}{3}\sigma_{ii}\delta\varepsilon_{jj}^{\mathrm{p}}\right)\mathrm{d}V = \int_S \left[\widehat{T}_i\delta u_i + \widehat{R}_i D(\delta u_i)\right]\mathrm{d}S + \sum_n \oint_{C_n} p_i\delta u_i\,\mathrm{d}C_n\,, \tag{11}$$

provided that the equations of equilibrium hold

$$\sigma_{ij,j} = 0\,, \quad \tau_{ijk,k} + \sigma_{ij} - q_{ij} = 0\,, \tag{12}$$

together with the relations

$$T_i = \sigma_{ij}n_j\,, \quad t_{ij} = \tau'_{ijk}n_k \tag{13}$$

between the traction vector T_i and the Cauchy stress tensor σ_{ij}, and between the (deviatoric) moment-traction tensor t_{ij} are the deviatoric part of the moment-stress tensor τ'_{ijk}. The components of the outward unit vector, orthogonal to the considered surface element, are denoted by n_i, and u_i are the displacement components.

The three independent traction components $\widehat{T}_i$ are

$$\widehat{T}_i = \overline{T}_i - n_i n_j R_j(D_k n_k) - D_i(n_j R_j)\,, \tag{14}$$

with

$$\overline{T}_i = T_i + R_i(D_j n_j) - D_j t_{ij}\,, \quad T_i = \sigma_{ij}n_j\,, \tag{15}$$

while the two independent higher-order traction components $\widehat{R}_i$, tangential to S, are

$$\widehat{R}_i = R_i - n_i n_j R_j\,, \quad R_i = t_{ij}n_j\,, \tag{16}$$

with $t_{ij} = \tau'_{ijk}n_j n_k$. The utilized surface gradient operator is defined

by $D_i = (\partial/\partial x_i) - n_i D$, where D is the projection of the gradient operator to the surface normal, $D = n_j(\partial/\partial x_j)$. The spherical component of Cauchy stress $\sigma_{ii}/3$ was used in (11) as the Lagrange multiplier, associated with the incompressibility constraint $\varepsilon^{\rm p}_{jj} = 0$ (Fleck and Willis, 2009b).

The line forces along the edges C_n of the smooth parts S_n of a piece-wise smooth surface S are denoted in (11) by p_i. For example, the line force along an edge formed by the intersection of two smooth surface segments $S^{(1)}$ and $S^{(2)}$ is

$$p_i = \left[\tau'_{ijk}k^{(1)}_j n^{(1)}_k - k^{(1)}_i \tau'_{jkl} n^{(1)}_j n^{(1)}_k n^{(1)}_l\right] + \left[\tau'_{ijk}k^{(2)}_j n^{(2)}_k - k^{(2)}_i \tau'_{jkl} n^{(2)}_j n^{(2)}_k n^{(2)}_l\right], \tag{17}$$

where $\mathbf{n}^{(i)}$ is the unit outward normal to surface $S^{(i)}$ $(i = 1, 2)$, and $\mathbf{k}^{(i)} = \mathbf{c}^{(i)} \times \mathbf{n}^{(i)}$. The vector $\mathbf{c}^{(i)}$ is the unit tangent vector along the intersecting edge of two surfaces, with $S^{(i)}$ to the left. The first subscript in τ_{ijk} specifies the normal to the surface over which the τ_{ijk} component acts, the second index specifies the orientation of the forces, and the third index specifies the orientation of the lever arm between the two forces of the doublet. Details of the derivation of (11)–(17) can be found in Lubarda (2016b).

The deviatoric parts of the microstress q_{ij} and the moment-stress τ_{ijk} are defined by

$$q'_{ij} = q_{ij} - \frac{1}{3}\, q_{kk}\delta_{ij}\,, \quad \tau'_{ijk} = \tau_{ijk} - \frac{1}{3}\,\tau_{llk}\delta_{ij}\,. \tag{18}$$

The spherical part of Cauchy stress tensor is usually specified from the equilibrium conditions in conjunction with the traction boundary conditions. The workless spherical parts of the microstress and the moment-stress tensor are included in the analysis for the convenience, and are related to the spherical part of Cauchy stress by $\tau_{jjk,k} + \sigma_{jj} - q_{jj} = 0$.

5. Bending of a prismatic beam

The effects of strain-gradients on plastic response have been studied for various problems at micron scale, including bending and torsion of thin beams and wires, plastic void growth, and indentation hardness testing (Fleck et al., 1994; Stölken and Evans, 1998; Gao et al., 1999; Nix and Gao, 1998; Huang et al., 2000; Haque and Saif, 2003; Shrotriya et al., 2003; Gudmundson, 2004; Lou et al., 2006; Evans and Hutchinson, 2009; Idiart et al., 2009; Polizzotto, 2011; Chen and Feng, 2011; Liu et al., 2013; Bardella and Panteghini, 2015; Lubarda, 2016a,b). In the bending analysis of ultra thin nickel beams, Stölken and Evans (1998) observed a strong size effect; 12.5 μm thick beams showed much stronger plastic work hardening than 100 μm thick beams. Their model was a plane-strain model with zero imposed strain in the direction of the width of the beam, as also used by Evans and Hutchinson (2009). Such model is addressed in Section 8 of this paper. In this section we consider pure bending of a rigid-plastic prismatic beam of length L, having a rectangular cross-section of width b and height h (Fig. 1). The applied bending moment at the ends of the beam $(x_1 = \pm L/2)$ is M. The corresponding curvature is $\kappa = 1/\rho$, where ρ is the radius of the curvature, so that the two ends of the beam rotate relative to each other by $L\kappa$. If the applied moment is greater than the yield-threshold moment $(M > M_Y)$, the non-vanishing strains are

$$\varepsilon_{11} = \kappa x_2\,, \quad \varepsilon_{22} = \varepsilon_{33} = -\frac{1}{2}\,\varepsilon_{11}\,, \tag{19}$$

with the corresponding gradients

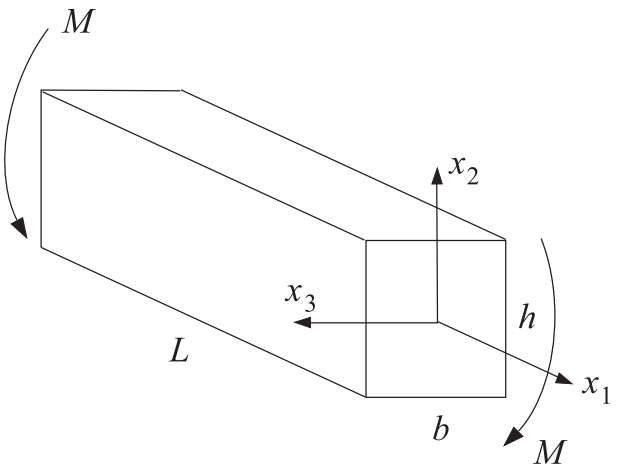

Fig. 1. The beam of length L and a rectangular cross-section of dimensions $b \times h$ under the bending moment M. The axis x_1 passes through the centroids of the cross-sections, and the axes (x_2, x_3) are as shown.

$$\varepsilon_{11,2} = \kappa\,, \quad \varepsilon_{22,2} = \varepsilon_{33,2} = -\frac{1}{2}\,\varepsilon_{11,2}\,. \tag{20}$$

The expression for M_Y will be derived in the sequel. The displacement fields is

$$u_1 = \kappa x_1 x_2\,, \quad u_2 = -\frac{1}{2}\,\kappa x_1^2 - \frac{1}{4}\,\kappa\left(x_2^2 - x_3^2\right), \quad u_3 = -\frac{1}{2}\,\kappa x_2 x_3\,. \tag{21}$$

The anticlastic curvature is $\widehat{\kappa} = \kappa/2$, so that the sides of the beam $x_3 = \pm b/2$ rotate relative to each other by $b\widehat{\kappa}$.

Since elastic component of strain is absent in the case of a rigid-plastic model, there is no deformation for $M \le M_Y$, while for $M > M_Y$ the entire deformation is plastic. Assuming proportional straining and the framework of the deformation theory of strain-gradient plasticity from Sections 2–4, we find from (3),

$$e_{\rm p} = \left(\frac{2}{3}\,\varepsilon^{\rm p}_{ij}\varepsilon^{\rm p}_{ij}\right)^{1/2} = \kappa|x_2|\,, \quad g_{\rm p} = \left(\frac{2}{3}\,\varepsilon^{\rm p}_{ij,k}\varepsilon^{\rm p}_{ij,k}\right)^{1/2} = \kappa\,. \tag{22}$$

Upon substitution of (22) into (2), the gradient-enhanced effective plastic strain becomes

$$E_{\rm p} = \kappa\left(|x_2|^s + l^s\right)^{1/s}. \tag{23}$$

For any κ, the entire contribution to $E_{\rm p}$ along $x_2 = 0$ plane is from the strain-gradient. As x_2 increases in magnitude the strain contribution increases, while the strain-gradient contribution remains constant. If $l \ll h$, the strain contribution in the outer portions of the beam (near $x_2 = \pm h/2$) is a dominant contribution to $E_{\rm p}$.

The deviatoric parts of the microstress and the moment-stress components can be determined by introducing (23) into (10). This gives

$$q'_{11} = \frac{2\sigma_0(E_{\rm p})}{3}\,\frac{|x_2|^{s-1}\,{\rm sign}(x_2)}{\left(|x_2|^s + l^s\right)^{1-1/s}}\,, \quad q'_{22} = q'_{33} = -\frac{1}{2}\,q'_{11}\,, \tag{24}$$

$$\tau'_{112} = \frac{2\sigma_0(E_p)}{3}\,\frac{l^s}{(|x_2|^s + l^s)^{1-1/s}}\,, \quad \tau'_{222} = \tau'_{332} = -\frac{1}{2}\,\tau'_{112}\,. \tag{25}$$

The deviatoric part of the Cauchy stress follows from the second equilibrium condition in (11) as

$$\sigma'_{11} = q'_{11} - \tau'_{112,2}\,, \quad \sigma'_{22} = \sigma'_{33} = -\frac{1}{2}\,\sigma'_{11}\,. \tag{26}$$

After evaluating $\tau'_{112,2}$ from (25), we obtain

$$\tau'_{112,2} = \frac{2}{3}\,\frac{l^s\big|x_2\big|^{s-1}\mathrm{sign}(x_2)}{(|x_2|^s + l^s)^{2-1/s}}\left[E_p\,\frac{d\sigma_0}{dE_p} - (s-1)\sigma_0(E_p)\right], \tag{27}$$

and the substitution into (26) gives

$$\sigma'_{11} = \frac{2}{3}\,\frac{\big|x_2\big|^{s-1}\mathrm{sign}(x_2)}{(|x_2|^s + l^s)^{2-1/s}}\left[(|x_2|^s + sl^s)\sigma_0(E_p) - l^s E_p\,\frac{d\sigma_0}{dE_p}\right],$$
$$\sigma'_{22} = \sigma'_{33} = -\frac{1}{2}\,\sigma'_{11}\,. \tag{28}$$

5.1. Boundary conditions and spherical parts of stress tensors

The equilibrium equation $\sigma_{22,2} = 0$ requires that $\sigma_{22} = \text{const.}$, and from the boundary condition $\sigma_{22}(x_2 = \pm h/2) = 0$ it follows that $\sigma_{22} = 0$ in the entire beam. This specifies the spherical part of the Cauchy stress, such that

$$\sigma'_{22} + \frac{1}{3}\,\sigma_{kk} = 0 \quad \Rightarrow \quad \frac{1}{3}\,\sigma_{kk} = -\sigma'_{22} = \frac{1}{2}\,\sigma'_{11}\,. \tag{29}$$

Consequently, the normal stress components within the beam are

$$\sigma_{11} = \frac{3}{2}\,\sigma'_{11} = \frac{\big|x_2\big|^{s-1}\mathrm{sign}(x_2)}{(|x_2|^s + l^s)^{2-1/s}}\left[(|x_2|^s + sl^s)\sigma_0(E_p) - l^s E_p\,\frac{d\sigma_0}{dE_p}\right],$$
$$\sigma_{22} = \sigma_{33} = 0\,. \tag{30}$$

The lateral surfaces of the beam are traction-free, and we require that $\tau_{222} = 0$ at $x_2 = \pm h/2$ and $\tau_{332} = 0$ at $x_3 = \pm b/2$. Both are fulfilled by defining the spherical part of the moment-stress τ_{ijk} such that

$$\tau_{222} = \tau'_{222} + \frac{1}{3}\,\tau_{pp2} = 0 \quad \Rightarrow \quad \frac{1}{3}\,\tau_{pp2} = -\tau'_{222} = \frac{1}{2}\,\tau'_{112}\,. \tag{31}$$

Consequently, the moment-stress components within the beam are

$$\tau_{112} = \frac{3}{2}\,\tau'_{112} = \sigma_0(E_p)\,\frac{l^s}{(|x_2|^s + l^s)^{1-1/s}}\,, \quad \tau_{222} = \tau_{332} = 0\,. \tag{32}$$

Finally, we specify the spherical part of the microstress q_{ij} as $(1/3)q_{kk} = -q'_{22}$ so that $q_{22} = q_{33} = 0$. The corresponding microstress field is then

$$q_{11} = \frac{3}{2}\,q'_{11} = \sigma_0(E_p)\,\frac{\big|x_2\big|^{s-1}\mathrm{sign}(x_2)}{(|x_2|^s + l^s)^{1-1/s}}\,, \quad q_{22} = q_{33} = 0\,. \tag{33}$$

In particular, the so-defined components σ_{11}, q_{11} and τ_{112} are related by

$$\sigma_{11} = q_{11} - \tau_{112,2}\,. \tag{34}$$

The results are particularly simple in the case $s = 1$; the derived expressions reduce to

$$q_{11} = \sigma_0(E_p)\mathrm{sign}(x_2)\,, \quad \tau_{112} = l\sigma_0(E_p)\,, \quad E_p = \kappa(|x_2| + l)\,, \tag{35}$$

$$\sigma_{11} = \left[\sigma_0(E_p) - l\kappa\,\frac{d\sigma_0}{dE_p}\right]\mathrm{sign}(x_2)\,. \tag{36}$$

Fig. 2 shows the variation of the normal stress σ_{11} (black curves) and microstress q_{11} (red curves) with x_2 at three levels of the surface strain $\varepsilon = h\kappa/2$. Part (a) is for $s = 1$, and part (b) for $s = 2$. The utilized stress-strain relationship is

$$\sigma_0(E_p) = \sigma_Y^0\left(1 + \frac{m}{n}E_p\right)^n\,, \tag{37}$$

where the initial yield stress is σ_Y^0, and the initial hardening rate $h_p = m\sigma_Y^0$. The material parameters are adjusted so that the initial hardening rate is $h_p = 46.66\sigma_Y^0$, while $\sigma_0(0.1) = 2\sigma_Y^0$. The latter is approximately an increase of stress due to hardening in polycrystalline copper after 10% strain; see experimental data reported in Fleck et al. (1994) and Liu et al. (2013). The material length parameter is chosen to be $l = h/4$ for all curves. The corresponding plots of the moment-stress τ_{112} are shown in Fig. 3. For $s = 1$, the moment-stress τ_{112} increases with $|x_2|$ (for $\kappa > 0$), while for $s = 2$ the moment-stress τ_{112} is a decreasing function of $|x_2|$, with the vanishing slope at $x_2 = 0$. As a consequence, the stress σ_{11} is smaller in magnitude than the microstress q_{11} in the case $s = 1$, but greater than q_{11} in the case $s = 2$. Furthermore, the stresses σ_{11} and q_{11} in the case $s = 2$ are zero at $x_2 = 0$, while in the case $s = 1$ they experience a discontinuity at $x_2 = 0$. For $s = 1$ and $\kappa = 0$ the Heaviside-type stress behavior resembles the ultimate (limit) state from the classical ideal plasticity. The variations of the stress components with x_2 for $s > 2$ can be more complex.

5.2. Line forces

For a rigid-plastic incompressible material, there is a line force along the upper and lower edge of the cross-section of the beam ($x_2 = \pm h/2$). It readily follows from (17) that along the upper edge ($x_2 = h/2$),

$$p_1 = (\tau'_{112} - \tau'_{222})_{x_2 = h/2} = \frac{3}{2}\,(\tau'_{112})_{x_2 = h/2} = (\tau_{112})_{x_2 = h/2}. \tag{38}$$

The result that $p_1 = \tau_{112}$ along the edge $x_2 = h/2$ could have been recognized from the outset by the basic equilibrium consideration: the sum of q_{11} and $-\tau_{112,2}$ give rise to σ_{11} at any point of the cross-section, see (34), while the edge value of τ_{112} gives rise to p_1. Consequently, by using (25) or (32), we obtain from (38),

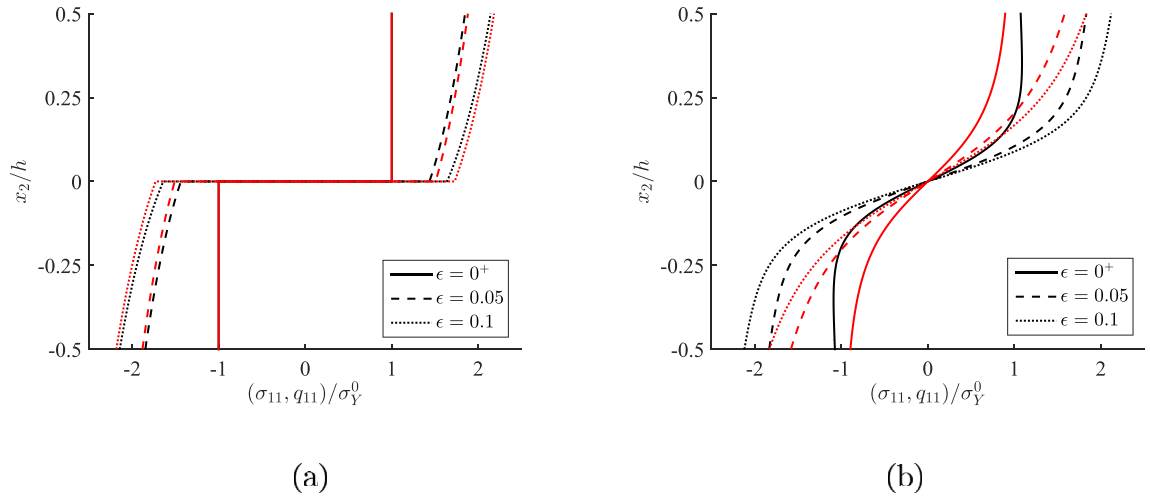

Fig. 2. The variations of σ_{11} (black curves) and q_{11} (red curves) with x_2/h at three levels of surface strain $\epsilon = h\kappa/2$. The relationship $\sigma_0 = \sigma_0(E_p)$ is specified by (37), with $m = 46.66$ and $n = 0.225$. The material length parameter is $l = h/4$. Part (a) is for $s = 1$, and part (b) for $s = 2$. (For interpretation of the references to colour in this figure legend, the reader is referred to the web version of this article.)

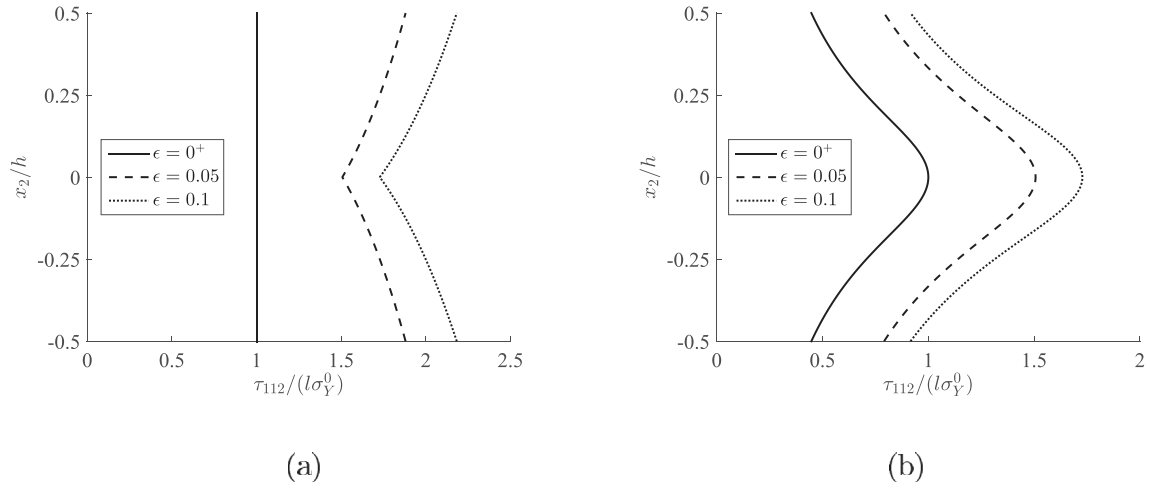

Fig. 3. The variation of τ_{112} with x_2/h at three levels of surface strain $\epsilon = h\kappa/2$ and the same data as used in Fig. 2. Part (a) is for $s = 1$, and part (b) for $s = 2$.

$$p_1 = \sigma_0\left(E_p^*\right)\frac{l^s}{\left[(h/2)^s + l^s\right]^{1-1/s}}, \quad E_p^* = \kappa\left[(h/2)^s + l^s\right]^{1/s}. \tag{39}$$

The same but opposite line force acts along the lower edge of the beam ($x_2 = -h/2$). These line forces are peculiar feature of the rigid-plastic strain-gradient model. If the elastic-plastic model was used instead, the line forces would be absent, but the elastoplastic solution would give rise to a rapidly increasing stress in boundary layers near the top and bottom edge. In the limit as the modulus of elasticity $E \to \infty$, these boundary layers of rapidly increasing stress give rise to line forces of the rigid-plastic model. Detailed numerical study of this transition has been performed by Engelen et al. (2006). The latter authors also derived an analytical closed form solution for the elastoplastic bending problem in the case of incompressible elastic response and a constant hardening modulus.

Regarding the boundary tractions $\widehat{T}_i$ and $\widehat{R}_i$ from Section 4, the only nonvanishing component is $\widehat{T}_1 = \sigma_{11}$, acting over the ends of the beam $x_1 = \pm L/2$.

6. Bending moment-curvature relationship

The bending moment required to produce a given curvature κ can be obtained from the overall moment-equilibrium condition. If the Cauchy stress σ_{11} and the line force p_1 are used, the expression is

$$M(\kappa) = 2b\int_0^{h/2} \sigma_{11}x_2\,\mathrm{d}x_2 + bhp_1. \tag{40}$$

If the equipollent stress system, consisting of the microstress q_{11} and the moment-stress τ_{112} is used instead, the expression is

$$M(\kappa) = 2b\int_0^{h/2} (q_{11}x_2 + \tau_{112})\,\mathrm{d}x_2. \tag{41}$$

The equivalency of the two expressions can be easily demonstrated by substituting (34) into (40) and by applying the integration by parts. An equivalent expression can also be derived by

equating the rate of internal work (per unit length of the beam) to the rate of external work, as done by Idiart et al. (2009). This gives

$$M\dot{\kappa} = 2b\int_0^{h/2}\left(q'_{ij}\dot{\varepsilon}^{\mathrm{p}}_{ij} + \tau'_{ijk}\dot{\varepsilon}^{\mathrm{p}}_{ij,k}\right)\mathrm{d}x_2 = 3b\dot{\kappa}\int_0^{h/2}(q'_{11}x_2 + \tau'_{112})\mathrm{d}x_2. \tag{42}$$

Since $q'_{11} = (2/3)q_{11}$ and $\tau'_{112} = (2/3)\tau_{112}$, upon the cancelation of $\dot{\kappa}$, (42) reproduces (41).

We proceed with the derivation of the expression for $M(\kappa)$ by using (41). From (32) and (33), we have in the upper portion of the beam ($0 \le x_2 \le h/2$),

$$q_{11} = \sigma_0(E_{\mathrm{p}})\,\frac{x_2^{s-1}}{(x_2^s + l^s)^{1-1/s}}\,, \quad \tau_{112} = \sigma_0(E_{\mathrm{p}})\,\frac{l^s}{(x_2^s + l^s)^{1-1/s}}. \tag{43}$$

The substitution of (43) into (41) gives

$$M(\kappa) = 2b\int_0^{h/2}(x_2^s + l^s)^{1/s}\sigma_0(E_{\mathrm{p}})\,\mathrm{d}x_2. \tag{44}$$

The corresponding rate of the bending moment with respect to the curvature is

$$\frac{\mathrm{d}M}{\mathrm{d}\kappa} = 2b\int_0^{h/2}(x_2^s + l^s)^{2/s}\,\frac{\mathrm{d}\sigma_0}{\mathrm{d}E_{\mathrm{p}}}\,\mathrm{d}x_2. \tag{45}$$

The yield-threshold moment for the onset of plastic deformation at $\kappa = 0$ is

$$M_Y = 2b\sigma_Y^0\int_0^{h/2}(x_2^s + l^s)^{1/s}\,\mathrm{d}x_2. \tag{46}$$

The yield-threshold moment in the absence of strain gradient effect ($l = 0$) is $M_Y^0 = \sigma_Y^0 bh^2/4$, regardless of s.

The right-hand sides of (44)–(46) can be evaluated numerically for any s and for any assumed relationship $\sigma_0 = \sigma_0(E_{\mathrm{p}})$. The results for $s = 1$ can be obtained analytically in a simple closed-form, as shown in Section 7. For some forms of the function $\sigma_0 = \sigma_0(E_{\mathrm{p}})$ there is also an analytical but more involved solution for $s = 2$ (in terms of the hypergeometric series, Idiart et al., 2009), but this will not be pursued here. Instead, the results for $s = 2$ presented in Section 7 are obtained by the direct numerical integration of (44), with the adopted relationship (37) for $\sigma_0 = \sigma_0(E_{\mathrm{p}})$. For linear hardening, closed-form solutions for $s = 1$ and $s = 2$ are given in the next section.

6.1. Linear hardening

In their experimental and analytical study of plasticity length scale effects in microbend testing of thin nickel foils, Stölken and Evans (1998) reported a measured tensile stress-strain curves with essentially linear strain hardening. Consequently, we derive in this section the moment-curvature relationship in the case when

$$\sigma_0(E_{\mathrm{p}}) = \sigma_Y^0(1 + kE_{\mathrm{p}}), \quad (k = \text{const.}). \tag{47}$$

The substitution of (47) into (44) gives

$$M(\kappa) = 2b\sigma_Y^0\int_0^{h/2}(x_2^s + l^s)^{1/s}\,\mathrm{d}x_2 + 2b\sigma_Y^0 k\kappa\int_0^{h/2}(x_2^s + l^s)^{2/s}\,\mathrm{d}x_2. \tag{48}$$

In the cases $s = 1$ and $s = 2$, the integration in (48) can be performed in closed-form. The results are

$$\frac{M(\kappa)}{M_Y^0} = 1 + 4(l/h) + \frac{1}{3}\,hk\kappa\left[1 + 6(l/h) + 12(l/h)^2\right], \quad (s = 1), \tag{49}$$

$$\frac{M(\kappa)}{M_Y^0} = \sqrt{1 + 4(l/h)^2} + 4(l/h)^2\sinh^{-1}(h/2l) + \frac{1}{3}\,hk\kappa\left[1 + 12(l/h)^2\right], \quad (s = 2). \tag{50}$$

Expressions (49) and (50) parallel expressions (14a) and (14b) of Stölken and Evans (1998), which were derived by using another version of the strain-gradient plasticity, with the separate length scales for the stretch and rotation gradients. Fig. 4a shows the variations of the yield-threshold value of the bending moment M_Y/M_Y^0, given by the right-hand sides of (49) and (50) when $\kappa = 0$. Fig. 4b shows the corresponding variations of the hardening rate $\mathrm{d}M/\mathrm{d}\kappa$.

7. Moment-curvature expressions for nonlinear hardening

If the stress-strain relationship from the uniaxial tension test is specified by (37), the moment-curvature expression (44) becomes

$$M(\kappa) = 2b\sigma_Y^0\int_0^{h/2}\left[1 + \frac{m\kappa}{n}(x_2^s + l^s)^{1/s}\right]^n(x_2^s + l^s)^{1/s}\,\mathrm{d}x_2. \tag{51}$$

In the case $s = 1$, (51) can be integrated to obtain

$$M(\kappa) = 2b\sigma_Y^0\left(\frac{n}{m\kappa}\right)^2\left(\frac{z^{n+2}}{n+2} - \frac{z^{n+1}}{n+1}\right)_{x_2=0}^{x_2=h/2}, \quad z = 1 + \frac{m\kappa}{n}\,(x_2 + l). \tag{52}$$

The corresponding yield-threshold moment (at $\kappa = 0$) is

$$M_Y = M_Y^0\left(1 + 4\,\frac{l}{h}\right), \quad M_Y^0 = \frac{1}{4}\,bh^2\sigma_Y^0\,. \tag{53}$$

Fig. 5a shows the variation of the normalized bending moment M/M_Y^0 with the surface strain $\varepsilon = \kappa h/2$ for three indicated values of l in the case $s = 1$. Fig. 5b shows the same in the case $s = 2$, which is obtained by numerical integration of (51). The nonlinear hardening was assumed with $m = 46.66$ and $n = 0.225$, as in Fig. 2. By comparing parts (a) and (b) it is observed that the increase of the material length l increases the moment significantly more in the case $s = 1$ than in the case $s = 2$. There is a strong effect of l on the initial yield strength; the smaller the ratio h/l, the higher the initial yield strength. There is a less pronounced increase of the hardening rate at larger values of ε with the increase of the ratio l/h. Experimental observations on nickel beams by Stölken and Evans (1998) indicate strong influence of the foil thickness on both the yield strength and the hardening rate. See also a related discussion by Evans and Hutchinson (2009), who extended the analysis to include the elastic component of strain and solved the governing equations of their model numerically.

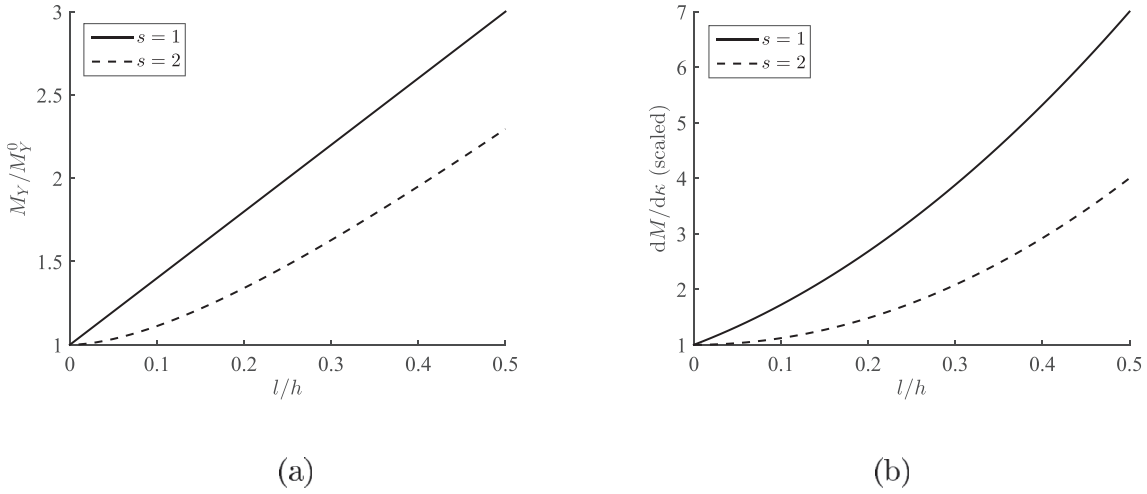

Fig. 4. (a) The variation of the normalized yield-threshold moment M_Y/M_Y^0 with l/h according to (47) for $s = 1$, and (48) for $s = 2$. (b) The variation of the corresponding hardening rate $\mathrm{d}M/\mathrm{d}\kappa$ (scaled by its value $khM_Y^0/3$ at $l = 0$).

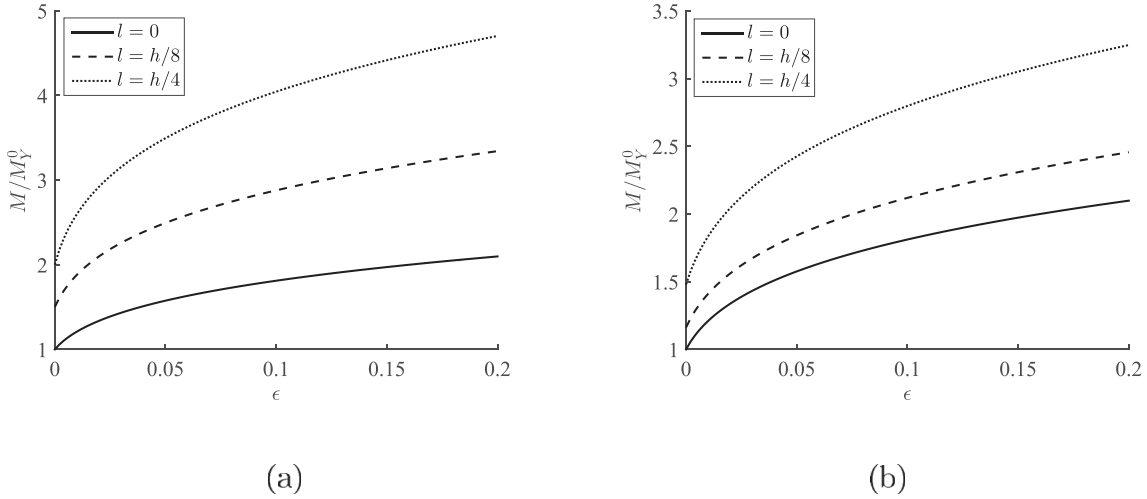

Fig. 5. The variation of the normalized moment M/M_Y^0 with the surface strain $\varepsilon = \kappa h/2$ for the three indicated values of l. (a) Case $s = 1$; (b) Case $s = 2$.

8. Rigid-plastic beam bending under plane-strain condition

The plane-strain approximation is commonly adopted in the bending analysis of wide thin beams (foils), e.g., Stölken and Evans (1998); Huang et al. (2000); Voyiadjis and Abu Al-Rub, 2005; Engelen et al. (2006); Idiart et al. (2009); Evans and Hutchinson (2009). The rationale for adopting the plane-strain approximation stems from the original microbent experimental setting by Stölken and Evans (1998), in which the foil was plastically bent around a small cylindrical mandril by means of loads applied through a profiled die. The anticlastic curvature was absent and the plane-strain conditions prevailed in the direction of the width of the foil, except near its ends. The objective in this section is to determine the stress fields and the moment-curvature relation, including the lateral moment required to prevent the anticlastic curvature and keep the plane-strain mode of the deformation. The height of the beam is again denoted by h, its width is $B \gg h$, and L is the length of the beam (Fig. 6).

Upon the onset of deformation, the non-vanishing strains are

$$\varepsilon_{11} = -\varepsilon_{22} = \kappa x_2\,, \quad \varepsilon_{33} = 0, \tag{54}$$

with the corresponding gradients

$$\varepsilon_{11,2} = -\varepsilon_{22,2} = \kappa\,, \quad \varepsilon_{33,2} = 0. \tag{55}$$

The displacement field is

$$u_1 = \kappa x_1 x_2\,, \quad u_2 = -\frac{1}{2}\,\kappa\left(x_1^2 + x_2^2\right), \quad u_3 = 0. \tag{56}$$

The anticlastic curvature is equal to zero, so that the rectangular cross-sections remain rectangular and of the same dimensions, experiencing only translation and rotation about their horizontal axis of symmetry (Fig. 6).

Since

$$e_{\mathrm{p}} = \left(\frac{2}{3}\,\varepsilon_{ij}^{\mathrm{p}}\varepsilon_{ij}^{\mathrm{p}}\right)^{1/2} = \frac{2}{\sqrt{3}}\,\kappa|x_2|\,, \quad g_{\mathrm{p}} = \left(\frac{2}{3}\,\varepsilon_{ij,k}^{\mathrm{p}}\varepsilon_{ij,k}^{\mathrm{p}}\right)^{1/2} = \frac{2}{\sqrt{3}}\,\kappa, \tag{57}$$

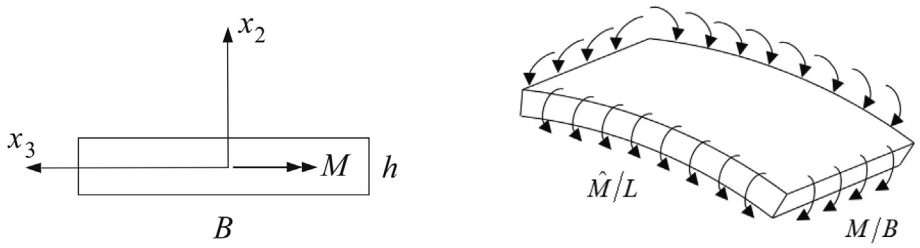

Fig. 6. (a) Cross-section of a thin wide beam of the thickness h and the width $B \gg h$. The applied bending moment is M. (b) The deformed shape of the beam under plane-strain in the x_3 direction. The applied bending moment per unit width of the beam is M/B. The lateral bending moment per unit length of the beam $\hat{M}/L$ is required to prevent the anticlastic curvature and ensure the plane-strain mode of deformation.

the gradient-enhanced effective plastic strain is

$$E_{\rm p} = \frac{2}{\sqrt{3}}\,\kappa\big(|x_2|^s + l^s\big)^{1/s}. \tag{58}$$

The only difference from the expression (23) of Section 5 is the presence of the coefficient $2/\sqrt{3}$ in (58).

The deviatoric parts of the microstress and the moment-stress are determined by introducing (58) into (10),

$$q'_{11} = -q'_{22} = \frac{\sigma_0(E_{\rm p})}{\sqrt{3}}\,\frac{|x_2|^{s-1}\,\mathrm{sign}(x_2)}{\big(|x_2|^s + l^s\big)^{1-1/s}}\,, \quad q'_{33} = 0. \tag{59}$$

$$\tau'_{112} = -\tau'_{222} = \frac{\sigma_0(E_{\rm p})}{\sqrt{3}}\,\frac{l^s}{\big(|x_2|^s + l^s\big)^{1-1/s}}\,, \quad \tau'_{332} = 0, \tag{60}$$

in agreement with expressions (40) and (41) from Idiart et al. (2009).

The deviatoric part of the Cauchy stress follows from (11) as

$$\sigma'_{11} = -\sigma'_{22} = q'_{11} - \tau'_{112,2}\,, \quad \sigma'_{33} = 0\,. \tag{61}$$

Upon evaluating $\tau'_{112,2}$ from (60), the substitution into (61) gives

$$\begin{aligned}\sigma'_{11} &= -\sigma'_{22}\\ &= \frac{1}{\sqrt{3}}\,\frac{|x_2|^{s-1}\,\mathrm{sign}(x_2)}{\big(|x_2|^s + l^s\big)^{2-1/s}}\left[\big(|x_2|^s + s l^s\big)\sigma_0(E_{\rm p}) - l^s E_{\rm p}\,\frac{{\rm d}\sigma_0}{{\rm d}E_{\rm p}}\right].\end{aligned} \tag{62}$$

8.1. Boundary conditions and spherical parts of stress tensors

The equilibrium equation $\sigma_{22,2} = 0$ requires that $\sigma_{22} = \text{const.}$, and from the boundary condition $\sigma_{22}(x_2 = \pm h/2) = 0$ it follows that $\sigma_{22} = 0$ in the entire beam. This specifies the spherical part of the Cauchy stress as

$$\frac{1}{3}\,\sigma_{kk} = -\sigma'_{22} = \sigma'_{11}. \tag{63}$$

Consequently, the non-vanishing stress components are

$$\begin{aligned}\sigma_{11} &= 2\sigma'_{11}\\ &= \frac{2}{\sqrt{3}}\,\frac{|x_2|^{s-1}\,\mathrm{sign}(x_2)}{\big(|x_2|^s + l^s\big)^{2-1/s}}\left[\big(|x_2|^s + s l^s\big)\sigma_0(E_{\rm p}) - l^s E_{\rm p}\,\frac{{\rm d}\sigma_0}{{\rm d}E_{\rm p}}\right],\\ \sigma_{33} &= \sigma'_{11} \equiv \frac{1}{2}\,\sigma_{11}.\end{aligned} \tag{64}$$

The lateral surfaces $x_2 = \pm h/2$ of the beam are traction-free, and we require that $\tau_{222} = 0$ there. Thus,

$$\tau_{222} = \tau'_{222} + \frac{1}{3}\,\tau_{pp2} = 0 \quad \Rightarrow \quad \frac{1}{3}\,\tau_{pp2} = -\tau'_{222} = \tau'_{112}. \tag{65}$$

The non-vanishing moment-stress components are accordingly

$$\begin{aligned}\tau_{112} &= 2\tau'_{112} = \frac{2}{\sqrt{3}}\,\sigma_0(E_{\rm p})\,\frac{l^s}{\big(|x_2|^s + l^s\big)^{1-1/s}}\,,\\ \tau_{332} &= \tau'_{112} \equiv \frac{1}{2}\,\tau_{112}\,.\end{aligned} \tag{66}$$

Therefore, while $\tau_{332} = 0$ in Section 5, see Eq. (32), in the plane-strain model $\tau_{332} \neq 0$, being associated with the constraint $\varepsilon_{33,2} = 0$. This is analogous to the presence of $\sigma_{33} \neq 0$, associated with the constraint $\varepsilon_{33} = 0$.

Finally, if the spherical part of the microstress is specified by $(1/3)q_{kk} = -q'_{22}$, then $q_{22} = 0$ and the non-vanishing microstress components are

$$q_{11} = 2q'_{11} = \frac{2}{\sqrt{3}}\,\sigma_0(E_{\rm p})\,\frac{|x_2|^{s-1}\,\mathrm{sign}(x_2)}{\big(|x_2|^s + l^s\big)^{1-1/s}}\,, \quad q_{33} = q'_{11} \equiv \frac{1}{2}\,q_{11}\,. \tag{67}$$

The so-specified components σ_{11}, q_{11} and τ_{112} are related by $\sigma_{11} = q_{11} - \tau_{112,2}$.

8.2. Line forces

From (17), the line force (per unit width of the beam) along the edge $x_2 = h/2$ is

$$p_1 = (\tau'_{112} - \tau'_{222})_{x_2 = h/2} = 2(\tau'_{112})_{x_2 = h/2} \equiv (\tau_{112})_{x_2 = h/2}. \tag{68}$$

Using (60) and (66), this gives

$$p_1 = \frac{2}{\sqrt{3}}\,\sigma_0\left(E_{\rm p}^*\right)\,\frac{l^s}{\left[(h/2)^s + l^s\right]^{1-1/s}}\,,$$
$$E_{\rm p}^* = \frac{2}{\sqrt{3}}\,\kappa\left[(h/2)^s + l^s\right]^{1/s}. \tag{69}$$

The same but opposite line force acts along the lower edge $x_2 = -h/2$.

The existence of line force p_1 in the rigid-plastic beam bending has been discussed by Engelen et al. (2006) in relation to elasto-plastic beam bending model by analyzing the features of elasto-plastic stress field in the limit of infinitely large modulus of elasticity. However, neither in that work nor in the related works by Huang et al. (2000) and Idiart et al. (2009), the line force p_3 along the intersection of the lateral sides $x_2 = \pm h/2$ and $x_3 = \pm B/2$, has been discussed. The determination of this force is important for the calculation of the lateral moment along the sides $x_3 = \pm B/2$ of the beam, required to cancel the anticlastic curvature of the beam along the edges $x_2 = \pm h/2$ and keep the plane-strain mode of the deformation. From (37), it follows that along the edge ($x_2 = h/2,\ x_3 = B/2 > 0$), the line force per unit length (L) of the beam is

$$p_3 = -\left(\tau'_{222}\right)_{x_2=h/2} \equiv \left(\tau_{332}\right)_{x_2=h/2}\,, \quad p_3 \equiv \frac{1}{2}\,p_1. \tag{70}$$

The same line force acts along the edge ($x_2 = -h/2,\ x_3 = -B/2$), and the opposite line force acts along the edges ($x_2 = -h/2,\ x_3 = B/2$) and ($x_2 = h/2,\ x_3 = -B/2$).

This derivation demonstrates the importance of the incorporation in the analysis of the spherical component of the moment-stress tensor τ_{ijk}, since this enables the fulfilment of the higher-order traction boundary conditions and the establishment of the expressions for the line forces $p_1 = (\tau_{112})_{x_2=h/2}$ and $p_3 = (\tau_{332})_{x_2=h/2}$, which have obvious physical interpretations, which are more clear than those following from their representations in terms of deviatoric parts of the moment-stress tensor, $p_1 = (\tau'_{112} - \tau'_{222})_{x_2=h/2}$ and $p_3 = -(\tau'_{222})_{x_2=h/2}$.

Regarding the boundary tractions $\widehat{T}_i$ and $\widehat{R}_i$ from Section 4, the only nonvanishing components are $\widehat{T}_1 = \sigma_{11}$ over the ends of the beam $x_1 = \pm L/2$, and $\widehat{T}_3 = \sigma_{33}$ over the lateral sides of the beam $x_3 = \pm B/2$.

8.3. Moment-curvature relationships

If the microstress q_{11} and the moment-stresses τ_{112} are used, the expression for the bending moment per unit width of the beam in the x_3 -direction is

$$\frac{M(\kappa)}{B} = 2\int_0^{h/2} \sigma_{11} x_2\,{\rm d}x_2 + h p_1 = 2\int_0^{h/2} (q_{11}x_2 + \tau_{112})\,{\rm d}x_2\,. \tag{71}$$

The substitution of (66) and (67) into (71) gives

$$\frac{M(\kappa)}{B} = \frac{4}{\sqrt{3}}\int_0^{h/2} \left(x_2^s + l^s\right)^{1/s}\sigma_0(E_{\rm p})\,{\rm d}x_2. \tag{72}$$

When $s = 2$, (72) reproduces the expression (31) from Idiart et al. (2009).

The yield-threshold moment (at $\kappa = 0$) is

$$\frac{M_Y}{B} = \frac{4\sigma_Y^0}{\sqrt{3}}\int_0^{h/2} \left(x_2^s + l^s\right)^{1/s}\,{\rm d}x_2. \tag{73}$$

The yield-threshold moment in the absence of the strain gradient effects ($l = 0$) is $M_Y^0/B = \sigma_Y^0 h^2/(2\sqrt{3})$.

The lateral moment (per unit length L of the beam), along the sides $x_3 = \pm B/2$, is

$$\frac{\widehat{M}(\kappa)}{L} = 2\int_0^{h/2} \sigma_{33}x_2\,{\rm d}x_2 + h p_3 = 2\int_0^{h/2} (q_{33}x_2 + \tau_{332})\,{\rm d}x_2. \tag{74}$$

Since $\sigma_{33} = \sigma_{11}/2$, $q_{33} = q_{11}/2$, and $\tau_{332} = \tau_{112}/2$, it readily follows that

$$\frac{\widehat{M}(\kappa)}{L} = \frac{1}{2}\,\frac{M(\kappa)}{B}. \tag{75}$$

No work is done by this lateral moment because the sides of the beam $x_3 = \pm B/2$ do not rotate in the plane-strain bending model. It may also be noted that (75) parallels the result from the elastic thin-plate theory: if there is no anticlastic curvature in a rectangular plate made of an incompressible material (Poisson's ratio $\nu = 1/2$), the bending moment (per unit length) along two parallel lateral sides is equal to one-half of the bending moment acting along the other two sides of the plate; see equation (b), page 289, of Timoshenko and Goodier (1970).

For the linear hardening with the stress-strain relation (47), the integral in (72) can be evaluated in closed-form for $s = 1$ and $s = 2$. The results are

$$\frac{M(\kappa)}{M_Y^0} = 1 + 4(l/h) + \frac{2}{3\sqrt{3}}\,hk\kappa\left[1 + 6(l/h) + 12(l/h)^2\right], \quad (s = 1), \tag{76}$$

$$\frac{M(\kappa)}{M_Y^0} = \sqrt{1 + 4(l/h)^2} + 4(l/h)^2 \sinh^{-1}(h/2l) + \frac{2}{3\sqrt{3}}\,hk\kappa\left[1 + 12(l/h)^2\right], \quad (s = 2). \tag{77}$$

Fig. 7 shows the variation of M/M_Y^0 with the surface strain

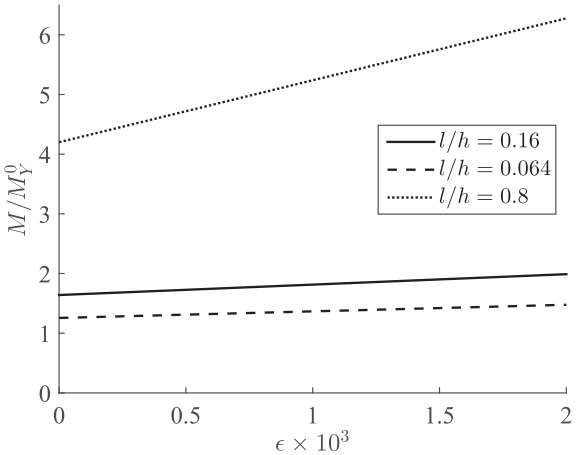

Fig. 7. The variation of M/M_Y^0 with the surface strain $\varepsilon = h\kappa/2$, according to (76). The hardening parameter is $k = 100$, and the utilized length scale $l = 8\ \mu$m.

$\varepsilon = h\kappa/2$, determined from (76). The hardening parameter $k = 100$ was used so that the tensile stress at the strain 2×10^{-3}, as determined from $\sigma_0 = \sigma_Y^0(1 + k\varepsilon_p)$, is 20% higher than the initial yield stress σ_Y^0, consistent with experimental data for polycrystalline Ni with the grain size of 27 μm and the yield stress $\sigma_Y^0 =$ 42 MPa (Ehrler et al., 2008; Evans and Hutchinson, 2009). The three lines shown in the plot correspond to indicated ratios l/h, which are obtained by taking the length parameter $l = 8$ μm, as in Evans and Hutchinson (2009), and the foil thickness $h = 10$, 50, and 125 μm, as used in experiments by Ehrler et al. (2008). The selected value of $l = 8$ μm makes the agreement between theoretical prediction and experimental data for $h = 50$ μm satisfactory, similar to agreement reported in Evans and Hutchinson (2009). The agreement is moderate for $h = 125$ μm, being better for larger strains, while for $h = 10$ μm the predicted values of M/M_Y^0 are too high, which indicates the limitation of the utilized strain-gradient plasticity model with only one length scale. For example, the predicted initial yield moment is about twice higher than experimentally observed value, while the hardening rate is lower than the values reported by Ehrler et al. (2008). This was further elaborated upon by Evans and Hutchinson (2009), who expanded their analysis to include a strain-dependent length scale, which improved the comparison with experimental data, as reported in their paper. Also, the thickness of the foil in the case $l/h = 0.8$ is only about one-third of the average grain size, which affected the predictions of the utilized model compared to experimental observations.

9. Conclusion

We have derived in this paper the expressions for the Cauchy stress, line forces, microstress, and moment-stress in prismatic beams of rectangular cross-section made of a rigid-plastic material. The model of strain-gradient plasticity with different measures of the gradient-enhanced effective plastic strain was used. The workless spherical parts of the microstress and the moment-stress tensors are included in the analysis and determined by fulfilling the higher-order traction boundary conditions. This was of importance for the determination of line forces and the derivation of the moment-curvature relationships. Closed-form analytical expressions for the latter are given in the case of linear hardening, and for some measures of the effective plastic strain in the case of nonlinear hardening. The analysis of the plane-strain bending of wide beams is then presented, since such model has been adopted in the bending analysis of thin foils. The line forces p_1 and p_3 are determined along the edges of the sides of the beam. They are used to derive the applied bending moment-curvature relationship $M = M(\kappa)$, and the lateral bending moment-curvature relationship $\widehat{M} = \widehat{M}(\kappa)$. The lateral stresses σ_{33}, q_{33}, and τ_{332} are found to be one-half of the corresponding longitudinal stresses σ_{11}, q_{11}, and τ_{112}. As a consequence, the lateral bending moment (per unit length of the beam) is equal to one-half of the applied bending moment (per unit width of the beam). The comparison to related work is given throughout the paper.

Acknowledgments

Research support from the Montenegrin Academy of Sciences and Arts is kindly acknowledged. I also thank the reviewers for their helpful comments and suggestions.

References

Anand, L., Gurtin, M.E., Lele, S.P., Gething, M., 2005. A one-dimensional theory of strain-gradient plasticity: formulation, analysis, numerical results. J. Mech. Phys. Solids 53, 1789–1826.
Bardella, L., 2006. A deformation theory of strain gradient crystal plasticity that accounts for geometrically necessary dislocations. J. Mech. Phys. Solids 54, 128–160.
Bardella, L., Panteghini, A., 2015. Modelling the torsion of thin metal wires by distortion gradient plasticity. J. Mech. Phys. Solids 78, 467–492.
Chen, S.H., Feng, B., 2011. Size effect in micro-scale cantilever beam bending. Acta Mech. 219, 291–307.
Ehrler, B., Hou, X.D., Zhu, T.T., P'Ng, K.M.Y., Walker, C.J., Bushby, A.J., Dunstan, D.J., 2008. Grain size and sample size interact to determine strength in a soft metal. Phil. Mag. 88, 3043–3050.
Engelen, R.A.B., Fleck, N.A., Peerlings, R.H.J., Geers, M.G.D., 2006. An evaluation of higher-order plasticity theories for predicting size effects and localisation. Int. J. Solids Struct. 43, 1857–1877.
Evans, A.G., Hutchinson, J.W., 2009. A critical assessment of theories of strain gradient plasticity. Acta Mater. 57, 1675–1688.
Fleck, N.A., Hutchinson, J.W., 1997. Strain gradient plasticity. Adv. Appl. Mech. 33, 295–361.
Fleck, N.A., Hutchinson, J.W., 2001. A reformulation of strain gradient plasticity. J. Mech. Phys. Solids 49, 2245–2271.
Fleck, N.A., Hutchinson, J.W., Willis, J.R., 2014. Strain gradient plasticity under non-proportional loading. Proc. Roy. Soc. A 470, 20140267.
Fleck, N.A., Hutchinson, J.W., Willis, J.R., 2015. Guidelines for constructing strain gradient plasticity theories. J. Appl. Mech. 82, 071002.
Fleck, N.A., Muller, G.M., Ashby, M.F., Hutchinson, J.W., 1994. Strain gradient plasticity: theory and experiment. Acta Metall. Mater. 42, 475–487.
Fleck, N.A., Willis, J.R., 2009. A mathematical basis for strain gradient plasticity theory. Part II: tensorial plastic multiplier. J. Mech. Phys. Solids 57, 1045–1057.
Gao, H., Huang, Y., Nix, W.D., Hutchinson, J.W., 1999. Mechanism-based strain gradient plasticity – I. Theory. J. Mech. Phys. Solids 47, 1239–1263.
Gudmundson, P.A., 2004. Unified treatment of strain gradient plasticity. J. Mech. Phys. Solids 52, 1379–1406.
Gurtin, M.E., Anand, L., 2005. A theory of strain-gradient plasticity for isotropic, plastically irrotational materials. Part I: small deformations. J. Mech. Phys. Solids 53, 1624–1649.
Gurtin, M.E., Anand, L., 2009. Thermodynamics applied to gradient theories involving accumulated plastic strain. The theories of Aifantis and Fleck and Hutchinson and their generalizations. J. Mech. Phys. Solids 57, 405–421.
Haque, M.A., Saif, M.T.A., 2003. Strain gradient effect in nanoscale thin films. Acta Mater. 51, 3053–3061.
Huang, Y., Gao, H., Nix, W.D., Hutchinson, J.W., 2000. Mechanism-based strain gradient plasticity - II. Analysis. J. Mech. Phys. Solids 48, 99–128.
Hutchinson, J.W., 2012. Generalizing J_2 flow theory: fundamental issues in strain gradient plasticity. Acta Mech. Sin. 28, 1078–1086.
Idiart, M.I., Deshpande, V.S., Fleck, N.A., Willis, J.R., 2009. Size effects in the bending of thin foils. Int. J. Eng. Sci. 47, 1251–1264.
Liu, D., He, Y., Dunstan, D.J., Zhang, B., Gan, Z., Hu, P., 2013. Toward a further understanding of size effects in the torsion of thin metal wires: an experimental and theoretical assessment. Int. J. Plast. 41, 30–52.
Lou, J., Shrotriya, P., Allameh, S., Buchheit, T., Soboyejo, W.O., 2006. Strain gradient plasticity length scale parameters for LIGA Ni MEMs thin films. Mater. Sci. Eng. A 441, 299–307.
Lubarda, V.A., 2016a. On the recoverable and dissipative parts of higher order stresses in strain gradient plasticity. Int. J. Plast. 78, 26–43.
Lubarda, V.A., 2016b. Rigid-plastic torsion of a hollow tube in strain-gradient plasticity. Int. J. Solids Struct. 100, 127–137.
Nielsen, K.L., Niordson, C.N., 2014. A numerical basis for strain gradient plasticity theory: rate-independent and rate-dependent formulations. J. Mech. Phys. Solids 63, 113–117.
Nix, W.D., Gao, H., 1998. Indentation size effects in crystalline materials: a law for strain gradient plasticity. J. Mech. Phys. Solids 46, 411–425.
Polizzotto, C., 2011. Size effects on the plastic collapse limit load of thin foils in bending and thin wires in torsion. Eur. J. Mech. A Solids 30, 854–864.
Shrotriya, P., Allameh, S.M., Lou, J., Buchheit, T., Soboyejo, W.O., 2003. On the measurement of the plasticity length scale parameter in LIGA nickel foils. Mech. Mater. 35, 233–243.
Stölken, J.S., Evans, A.G., 1998. A microbend test method for measuring the plasticity length scale. Acta Mater. 46, 5109–5115.
Timoshenko, S.P., Goodier, J.N., 1970. Theory of Elasticity. McGraw-Hill, New-York.
Voyiadjis, G.Z., Abu Al-Rub, R.K., 2005. Gradient plasticity theory with a variable length scale parameter. Int. J. Solids Struct. 42, 3998–4029.
Wang, W., Huang, Y., Hsia, K.J., Hu, K.X., Chandra, A., 2003. A study of microbend test by strain gradient plasticity. Int. J. Plast. 19, 365–382.